Visible and near-infrared organic photosensitizers comprising isoindigo derivatives as chromophores: synthesis, optoelectronic properties and factors limiting their efficiency in dye solar cells†

Cyril Aumaitre,[a] Cristina Rodriguez-Seco,[b] Jesús Jover,[b] Olivier Bardagot,[a] Florent Caffy,[a] Yann Kervella,[a] Nuria López,[b] Emilio Palomares *[bc] and Renaud Demadrille *[a]

The development of ruthenium-free organic photosensitizers showing panchromatic absorption up to the near-infrared (NIR) region for application in dye-sensitized solar cells (DSSCs) is still scarce. Among the sensitizers with absorption beyond 700 nm and developed for DSSCs, only zinc-phthalocyanine and boron-dibenzopyrromethene-based dyes have been able to reach efficiencies as high as 6%. Here we report metal-free organic dyes based on isoindigo, thieno-isoindigo or benzo-thieno-isoindigo chromophores that absorb in the UV-visible and NIR spectral range up to 900 nm. These molecules, that exhibit purple, blue, or green hues, were used to sensitize TiO_2 mesoporous electrodes in order to fabricate DSSCs with an iodide/triiodide-based electrolyte. Advanced photophysical characterizations, including charge extraction, transient photovoltage, and laser transient absorption spectroscopy experiments, combined with density functional theory modeling and computational investigations allow us to fully unravel the interfacial processes at the origin of the solar cell performances and to identify the limiting factors. A power conversion efficiency as high as 7% associated with a J_{sc} close to 19 mA cm^{-2} was obtained with one of the dyes, which is comparable to those of the best panchromatic organic dyes reported so far. We also demonstrate in this work that the V_{oc} of the solar cells is linearly correlated to the dipolar moments of the oxidized dyes, the molecules possessing larger dipoles leading to the highest V_{oc} values.

Introduction

Among the third generation photovoltaic technologies, dye-sensitized solar cells (DSSCs) show some of the required features for everyday life applications and a rapid development at the industrial level.[1] Indeed they can combine high efficiency[2] along with good stability,[3] and be semi-transparent and colorful, which are substantial advantages for building integrated photovoltaics (BIPVs).[4] For these reasons, they can be seen as a cost-effective alternative to conventional solar cells based on inorganic semi-conductors. For many years, ruthenium complexes have been developed and employed as sensitizers in DSSCs and photoconversion efficiencies (PCEs) up to 12% have been reported using them.[5] However, the scarcity and high price of ruthenium and the toxicity of some of its derivatives have pushed the scientific community to investigate other classes of sensitizers. Highly efficient molecules have emerged from this work such as zinc porphyrin dyes, which demonstrate efficiencies in solar cells that can reach 13%.[6] Nevertheless, other organic dyes based on various chromophores including quinoxaline derivatives,[7] benzothiadiazole,[8] or diketopyrrolopyrrole,[9] to name a few, have also shown impressive performances. In general, organic dyes show a D–π–A structure where the electron-donor unit (D) is, in most cases, a triarylamine group and the electron acceptor (A) unit is usually cyano-acrylic acid that also acts as a tether group. The choice of the π-conjugated linker in these molecules is critical since it influences the energy levels of the orbitals and governs the position of the intramolecular charge transfer (ICT) absorption band, which in turn determines the range of absorption and the color of the dye. It is still considered nowadays that some improvements in the efficiency of dye solar cells could come from the use of new photosensitizers with the condition that they possess a good absorption spectral match with the solar

[a]University Grenoble Alpes, CNRS, CEA, INAC, SyMMES, 17 rue des martyrs, F-38000, Grenoble, France. E-mail: renaud.demadrille@cea.fr

[b]Institute of Chemical Research of Catalonia (ICIQ), The Barcelona Institute of Science and Technology, Avenguda Països Catalans, 16, Tarragona, 43007, Spain. E-mail: epalomares@iciq.es

[c]ICREA, Passeig Lluís Companys, 23, Barcelona, E-08010, Spain

† Electronic supplementary information (ESI) available. See DOI: 10.1039/c8ta01826j

emission spectrum. Therefore, development of organic dyes showing wide absorption up to the near-IR range (so-called panchromatic dyes) is important to explore. Pioneering work in phthalocyanines for DSSCs, by Torres *et al.*, paved the way for solar cells with a near-IR response.[10] Yet, to date more than one thousand organic dyes have probably been synthesized and tested as sensitizers for TiO_2 with variable performances in solar cells, but only a small fraction of them show panchromatic absorption or have the ability to absorb photons up to the near-IR region.[11] Despite advantageous optical properties, only a few reach efficiencies close to 6%.[12]

One popular strategy to obtain organic dyes exhibiting broad absorption in the visible up to the near-IR relies on the use of motifs with a strong electron-withdrawing character in the backbone. The combination of such units with the electron-rich triarylamines gives rise to ICT absorption bands in the visible range whose position can be tuned depending on the strength of the electron-withdrawing blocks. Following this approach, in this work we have synthesized and used several isoindigo derivatives for the preparation of panchromatic sensitizers. Isoindigo is an isomer of the well-known natural and robust blue dye indigo. Isoindigo is particularly an interesting building block that shows a strong electron-withdrawing character due to the presence of two γ-lactam rings in the structure. Another interesting feature of this molecule is that it can be synthesized starting from natural synthons *i.e.* isatin. The isoindigo building block has already been investigated for the preparation of semiconducting polymers for bulk-heterojunction solar cells[13] or photosensitizers for DSSCs.[14] These dyes exhibit usually a broad absorption domain up to 750 nm but, in spite of this interesting characteristic, their photovoltaic efficiencies are between 3 and 7.5%.[15]

In the last decade, other isoindigo derivatives such as thieno-isoindigo or benzothieno-isoindigo have been successfully prepared to serve as building units in the preparation of low-band gap semiconducting copolymers,[16] showing a better absorption in the long wavelengths.[17] But surprisingly none of these synthons have been employed for the synthesis of dyes applicable in DSSCs. Although similar to isoindigo, thanks to their two lactam rings that ensure a strong electron-withdrawing character, these chromophores have terminations that differ in the nature of the side aromatic rings; in benzothieno-isoindigo, one phenyl is replaced by a thiophene and in thieno-isoindigo, two thiophene rings are present.

In this work, we report the synthesis of original organic dyes based on these three synthons. The molecules have been fully characterized by UV-Vis-NIR spectroscopy and electrochemistry prior to their use as photosensitizers in DSSCs. We show that swapping the isoindigo unit by a benzothieno-isoindigo or a thieno-isoindigo unit leads to a large shift of the absorption range toward the NIR part of the spectrum (up to 900 nm) with a simultaneous increase of the molar absorption coefficient (up to 44 000 M^{-1} cm^{-1}). The energy levels of the frontier orbitals have been determined by cyclic voltammetry (CV), differential pulse voltammetry (DPV) and estimated by Density Functional Theory (DFT) calculations. The consistent results indicate that the dyes can effectively be employed in a DSSC device to sensitize TiO_2 mesoporous electrodes with I^-/I_3^- as a redox mediator in the electrolyte. Photovoltaic properties of DSSCs based on this series of dyes have been investigated under simulated 1 sun AM 1.5 illumination and PCEs ranging from 0.45% to 5.84% have been measured. Charge extraction, transient photovoltage and transient absorption spectroscopy experiments have been carried out on these devices, and DFT modeling has been used to complete the study. This has allowed us to unravel the origin of the low J_{sc} and V_{oc} obtained with some of these compounds and the reasons behind their limited efficiencies. Taking into account this structure–property relationship and the detrimental identified phenomena that should be suppressed to improve their performances, we synthesized a new photosensitizer based on an isoindigo core and a modified triphenylamine (TPA) unit to decrease the recombination processes. This new panchromatic dye leads to devices with efficiency close to 7% associated with current densities above 19 mA cm^{-2} which ranks amongst the highest J_{sc} ever obtained for a panchromatic metal-free organic dye.

Results and discussion

Design and synthesis of the dyes

In the last decade, organic dyes with a D–π–A chemical structure have been widely developed due to their ability to foster the electron transfer within the dye towards the wide band gap semiconductor. Following this approach, the dyes of this study were synthesized by embedding the isoindigo, thieno-isoindigo of benzothieno-isoindigo units in between a donating segment based on triarylamine (D) and an electron accepting unit constituted by phenyl-cyanoacrylic acid (A). Two different triarylamines showing different electron donating strengths were used. The first one is a triphenylamine connected to an octylthiophene (TPAT8). This unit was initially developed in our laboratory to synthesize RK1, a dye that combines a high efficiency (over 10%) and an outstanding stability (T_{80} over 6000 h under an ISOS-L2 ageing test).[3a] The second triphenylamine unit that we employed consists of a fused triphenylamine with a thiophene through the formation of an indene ring (TPAF). The chemical structures and synthetic routes of the six dyes named **TPAT8-Iso**, **TPAT8-Altiso**, **TPAT8-Tiso**, **TPAF-Iso**, **TPAF-Altiso** and **TPAF-Tiso** are presented in Scheme 1. These dyes have been prepared following a common synthetic strategy. First, we synthesized the isoindigo, benzothieno-isoindigo or thieno-isoindigo cores *via* acid-promoted condensation starting from 6-bromoisatine, 6-bromooxindole, thieno-isatin, or thieno-oxindole. The attachment of branched alkyl chains on the nitrogen atoms of the lactam rings has been either performed directly on these precursors or on the formed cores. In the substitution process, 2-ethylhexyl side chains have been employed since they ensure a good solubility of the dyes in common organic solvents and they can help reducing dye aggregation once grafted onto the TiO_2 surface.[3c] Then the isoindigo, benzothieno-isoindigo or thieno-isoindigo cores have been coupled at one extremity to benzaldehyde *via* a Suzuki coupling reaction. The TPAT8 or TPAF donating units were coupled at the other extremity through a Stille coupling

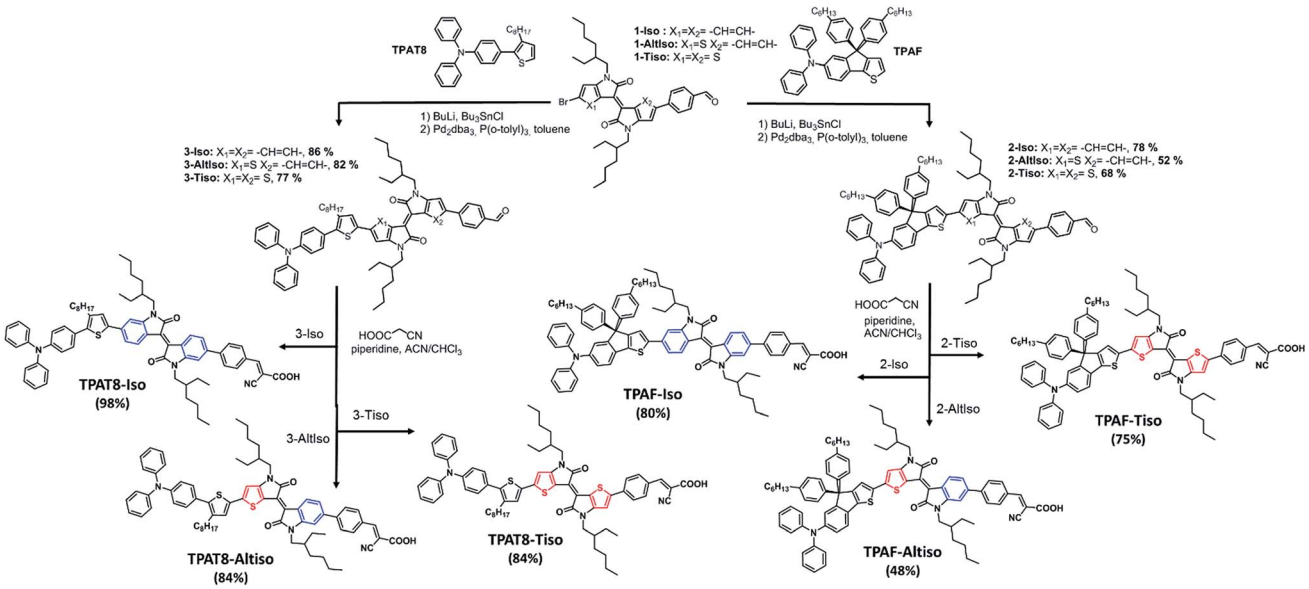

Scheme 1 Synthetic routes to the dyes TPAT8-Iso, TPAT8-Altiso, TPAT8-Tiso, TPAF-Iso, TPAF-Altiso and TPAF-Tiso.

reaction. The final dyes were then simply obtained from these aldehyde precursors by Knoevenagel condensation with cyano-acrylic acid. The preparation of all the precursors and all the dyes is fully described in the ESI.†

Optoelectronic and electrochemical properties

The absorption spectra of the isoindigo, benzothieno-isoindigo, or thieno-isoindigo based dyes were recorded in CH_2Cl_2 and as adsorbed onto 2 μm-thick TiO_2 films with chenodeoxycholic acid (CDCA). This co-adsorbent was used to reproduce the real conditions of use (see Fig. 1). The absorption wavelengths, molar extinction coefficients, and HOMO–LUMO energy levels of the six dyes are summarized in Table 1. The UV-vis spectra in solution exhibit two major bands, one appearing at 355–410 nm and the other prominent one at 575–740 nm. The former can be attributed to the π–π* transitions from the different aromatic rings being in conjugation. The absorption band at 575–740 nm may be attributed to the ICT transition from the triarylamine donor group to the isoindigo derivative cores connected to the cyano-acrylic acceptor unit. As expected, replacing the TPAT8 donor group by a fused unit, such as TPAF, results in a bathochromic spectral shift of the ICT band (by 30–40 nm depending on the core). More strikingly, the modification of the core itself, *i.e.* replacing the phenyl groups in the isoindigo structure by thiophene rings, has a huge impact on the position and the absorption coefficient of this band. Indeed, the maximum wavelength of absorption shifts toward the near-infrared leading to dyes revealing a purple, blue or green hue (see Fig. 1). For instance, the λ_{max} of the ICT band of **TPAF-Tiso** is red-shifted by 129 nm compared to that of **TPAF-Iso**. Interestingly, the molar extinction coefficient of this band also rises to attain 44 000 M^{-1} cm^{-1}. To summarize, swapping one or two benzene rings in the isoindigo core by one or two thiophene rings induces bathochromic and hyperchromic effects on the ICT band and, consequently, the percentage of absorption of the dyes in the near-infrared region is increased to reach a maximum rate of 35%. This value corresponds to the ratio of absorption above 700 nm divided by the overall absorption. Compared with the solution spectra, the maximum absorption peaks of the dyes, registered on 2 μm-thick transparent TiO_2 films using CDCA as a co-adsorbent, shift to the blue by 25, 55, 81, 28, 55 and 65 nm for **TPAF-Iso**, **TPAF-Altiso**, **TPAF-Tiso**, **TPAT8-Iso**, **TPAT8-Altiso** and **TPAT8-Tiso**, respectively (Table 1).

Usually the blue-shift of λ_{max} going from solution to thin films may be partially attributed to the deprotonation of the carboxylic acid.[18] However this shift is far too large in our case to be solely explained by this phenomenon. Broader blue-shifts can be generally ascribed to the formation of H-aggregates.[19] Despite the fact that we employed CDCA in the dyeing solution and that we used branched alkyl chains to prevent such event, this is probably the case here. This phenomenon was already observed for isoindigo-based dyes,[14] nonetheless it should be noted that this effect is enhanced when one thiophene is introduced in the isoindigo core and even more pronounced when two thiophene rings are present. This can be rationally explained by the conformation of the molecules found with DFT calculations, in which the core of the molecule becomes more planar whenever a thiophene motif is embedded (see the ESI†). In spite of the aggregation, the dye spectra in the solid state are broader and all the dyes show a panchromatic absorption up to the NIR region with absorption edges ranging from 700 nm to *circa* 875 nm. To accurately investigate the chemical modification effects on the molecular energy levels, the electrochemical properties of these dyes were analyzed by cyclic voltammetry and differential pulse voltammetry in CH_2Cl_2 solution with 0.2 M tetrabutylammonium hexafluorophosphate ($TBAPF_6$). All potentials reported are referenced to an Fc^+/Fc redox couple as an internal standard. For comparison purpose, DFT calculations were performed in a CH_2Cl_2 solvent phase model to obtain

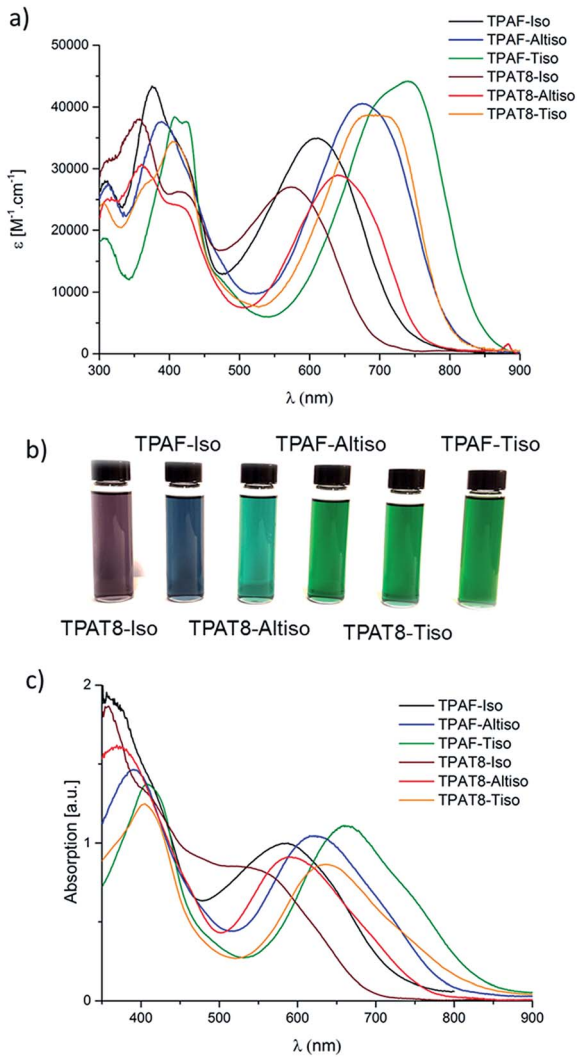

Fig. 1 (a) UV-Vis spectra of the dyes in dichloromethane, (b) pictures of the solutions and (c) UV-Vis spectra of the dyes recorded on TiO_2 films.

the derived HOMO and LUMO values and their respective spatial localizations (ESI†). All these data are summarized in Table 1 and Fig. 2. Consistent data were found for each dye from CV and DPV measurements. It is noteworthy that the mean values gathered from electrochemistry for the HOMO energy levels are in excellent agreement with the values determined by the DFT calculations.[20] The LUMO energy levels measured using electrochemistry are almost identical for all compounds (−3.7 to −3.8 eV) and a discrepancy of *circa* 0.3 eV is observed with the DFT computed values. This difference is not surprising since the vacant orbitals are generally more difficult to describe theoretically than the occupied ones.[21] It appears that the chemical variations either on the TPA unit or on the core of the molecules do not change the LUMO energy level positions. In contrast, some significant variations are observed for the HOMO energy levels which are all lying between −4.9 eV and −5.2 eV. Two effects can be commented; first, the replacement of the TPAT8 unit by a TPAF unit, which has a stronger electron donating character, induces a positive shift of 0.1 eV of the HOMO energy level position. Second, the HOMO energy level rises by 0.1 eV each time when a thiophene is introduced in the core. Our results are totally consistent with the work of Estrada *et al.* who demonstrated that the HOMO energy levels of compounds based on isoindigo derivatives are mainly influenced by the stilbene motif whereas the LUMO energy levels are mainly related to the fumaraldehyde motif present in the core structure.[22] As a consequence, the use of electron rich aromatic rings such as thiophene to replace benzene rings in isoindigo predominantly leads to the rise of the HOMO energy level.

The optimized molecular structures and isoelectronic densities are shown in Fig. 2. DFT calculations show that the HOMOs are localized at the TPAT8 or TPAF donor moieties and they extend to the core of the molecules. The delocalization of the HOMOs is not the same in all compounds. In isoindigo-based dyes, the HOMOs poorly overlap with the central core, whereas in benzothieno-isoindigo and thieno-isoindigo dyes, the HOMOs fully extend on these units.

To better explain this observation, the bond length alternation (BLA) of the chemical bonds located at each side of the cores was calculated. The BLA is between 0.059 and 0.076 Å in isoindigo dyes and it is the characteristic of aromatic systems. In benzothieno-isoindigo dyes, these distances decrease to attain values ranging from 0.037 to 0.064 Å and in thieno-

Table 1 Optical and electrochemical properties of isoindigo, benzothieno-isoindigo and thieno-isoindigo based dyes

	Optical properties					Electronic properties			
	λ_{max}-UV[a,b] [nm]	λ_{max}-Vis-NIR[a,b] [nm]	ε[a] [M^{-1} cm^{-1}]	λ_{onset}[a,b] [nm]	Abs (NIR)[a] (%)	ΔE_{opt}[c] [eV]	HOMO[d,e] [eV]	LUMO[d,e] [eV]	ΔE_{elec}[f] [eV]
TPAF-Iso	376 (355)	611 (586)	35 000	736 (750)	3	1.7	−5.1 (−5.2)	−3.8 (−3.3)	1.3
TPAF-Altiso	389 (391)	675 (620)	40 000	800 (800)	17	1.6	−5.0 (−5.1)	−3.7 (−3.3)	1.3
TPAF-Tiso	408 (408)	740 (659)	44 000	845 (875)	35	1.5	−4.9 (−5.0)	−3.7 (−3.4)	1.2
TPAT8-Iso	358 (355)	574 (546)	27 000	686 (700)	1	1.8	−5.2 (−5.3)	−3.7 (−3.4)	1.5
TPAT8-Altiso	361 (369)	645 (590)	33 500	757 (775)	7	1.6	−5.1 (−5.2)	−3.8 (−3.3)	1.3
TPAT8-Tiso	405 (405)	700 (635)	38 800	815 (850)	19	1.5	−5.0 (−5.1)	−3.7 (−3.4)	1.3

[a] Measured in CH_2Cl_2 at room temperature at a concentration of 10^{-5} M. [b] Parenthesis, measured after dyeing of 2 μm thick TiO_2 films on the glass substrate, in the presence of CDCA (dyeing solution 0.2 mM dye/2.0 mM CDCA). [c] Calculated from the optical absorption onset. [d] Mean values calculated from oxidative potential for the HOMO and reduction potential for the LUMO, measured by DPV and CV in CH_2Cl_2 (2×10^{-3} M) at room temperature, ferrocene/ferrocenium was used as the internal standard and measured at +0.48 V (−4.8 eV). [e] Parenthesis, determined by DFT calculations. [f] $\Delta E_{elec} = E_{LUMO} - E_{HOMO}$.

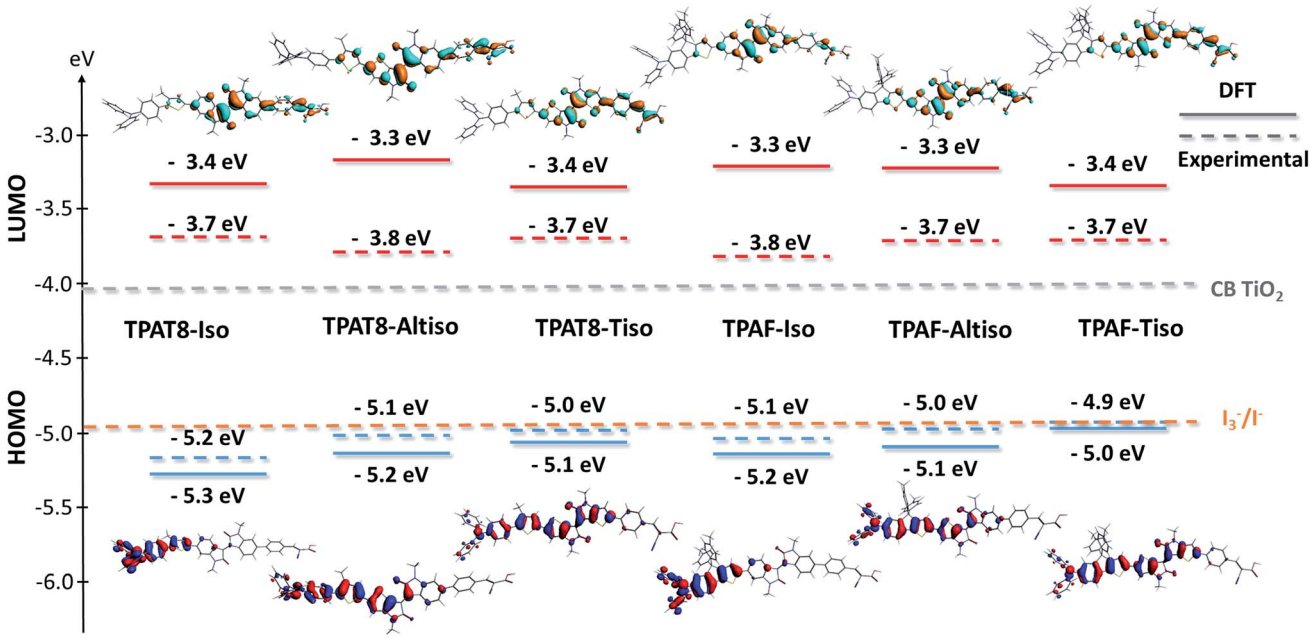

Fig. 2 Experimental and DFT calculated energy levels of the frontier orbitals of the dyes and their spatial localizations, conduction band (CB) of the TiO_2 and Nernst potential of the triiodide/iodide redox couple.

isoindigo-based molecules, the BLA is between 0.035 and 0.040 Å: these values are typical of quinoidal compounds,[23] which is in good agreement with the electrochemically and optically derived data. On the other hand, the LUMOs of the six molecules are primarily localized on the cores and the phenylcyanoacrylic acid unit. Such a directional electronic distribution is preferred for good electron injection into TiO_2 from dye anchoring sites.

To summarize this section, the six dyes present broad absorptions covering the solar spectrum from the UV to the NIR that could give rise to large photocurrents. Their LUMO energy levels positioned around −3.8 eV are located 0.25 eV above the energy level of the conducting band of the oxide (around −4.05 eV) which is the minimum driving force required to achieve an efficient injection of electrons in the oxide.[24] However, the experimentally estimated HOMO levels of the dyes, are between −5.2 eV and −4.9 eV. Some of them are very close to the Nernst potential of the triiodide/iodide-based redox electrolyte which is around −4.9 eV (*i.e.* 0.4 V *versus* NHE).[25] This means that for **TPAT8-Tiso**, **TPAF-Tiso**, **TPAT8-Altiso** and **TPAF-Altiso**, the ΔE_{reg} might not be sufficient to regenerate the oxidized species of the dyes. Finally, the larger overlap between HOMO and LUMO, deduced from the computed structures of these four dyes, might also be detrimental for the photocurrent generation.[26]

Photovoltaic properties

The performances of the DSSCs with these dyes were measured with a mask under an irradiation of AM 1.5 (1000 W m^{-2}) simulated solar light after calibration. For a direct comparison, we fabricated solar cells with the same photoelectrode composition consisting of a double layer TiO_2 (a 12 μm-thick transparent layer and a 4 μm-thick scattering layer) from Solaronix. This thickness was chosen taking into account a previous study that showed that thicker electrodes give higher photocurrent densities and performances.[3] This hypothesis was further confirmed through tests with some of our dyes (see the ESI†). Then, we started to optimize some of the fabrication parameters of the solar cells and we focused our preliminary investigations on the isoindigo dyes **TPAF-Iso** and **TPAT8-Iso**.

By analyzing the conclusion of several papers from the literature, we noticed that most of the devices comprising isoindigo-based sensitizers did not contain *tert*-butyl-pyridine (*t*BP) in the electrolyte.[14,15b,27] For other class of dyes, classical electrolytes contain 0.5 M of *t*BP. The reason behind this statement is the following: the LUMO energy level of the isoindigo dyes is usually close to the energy level of the CB of TiO_2, and *t*BP is known to shift the CB band of the oxide positively through a dipole effect.[28] By suppressing this dipole effect, the CB of TiO_2 is located at a lower energy level and the injection process is favored. On the other hand, the removal of *t*BP has a detrimental consequence on the V_{oc} of the solar cells, which becomes lower because the energy difference between this energy level and the redox potential of the electrolyte decreases. Consequently, an optimum concentration has to be found to obtain a good trade-off between J_{sc} and V_{oc}.

Several preliminary tests in solar cells using a dye/CDCA ratio of 0.2/2 mM were carried out with various amounts of *t*BP in the electrolyte or without *t*BP (see the ESI†), and we found that 0.1 M is an optimum concentration to reach the highest performances. We highlight within this first series of tests, the tremendous effect of this additive on the performances and the necessity to tune the formulation of the electrolyte with this class of dyes. Indeed, with a standard amount of *t*BP (0.5 M) the performances of **TPAF-Iso** and **TPAT8-Iso** are limited to 0.88%

and 1.27% with J_{sc} below 2.7 mA cm^{-2}, and the V_{oc} values are 0.64 and 0.61 V, respectively. When the concentration of *t*BP is lowered, the performances are better, and for an optimum concentration of 0.1 M, performances around 4% are achieved with J_{sc} reaching 9.6 mA cm^{-2} and 10.2 mA cm^{-2}. As expected, the V_{oc} of the resulting cells is slightly lower (around 0.55 V), but this loss is largely compensated by a more efficient injection process, which produces four times higher photocurrents. The strong influence of the *t*BP concentration on the performances further confirms that the LUMO energy levels of the dyes are close to the limit for an efficient electron injection.[26b]

From the UV-vis spectra of the molecules recorded on TiO_2 films (*vide supra*), we learned that our dyes have a large propensity to form aggregates even in the presence of CDCA. Aiming to reduce this dye aggregation, higher amounts, up to 12 mM of CDCA, were used in the dyeing bath of **TPAT8-Iso** for further tests, and the performances of the corresponding solar cells were measured. The *I–V* curves and photovoltaic parameters are given in the ESI.† When the concentration of the co-adsorbent is fixed between 10 and 12 mM, J_{sc} as high as 15.9 mA cm^{-2} is observed, leading to the PCE of up to 5.84%. Solar cells were fabricated with the six dyes under these optimized conditions; the *I–V* curves are presented in Fig. 3 and the corresponding photovoltaic parameters are summarized in Table 2.

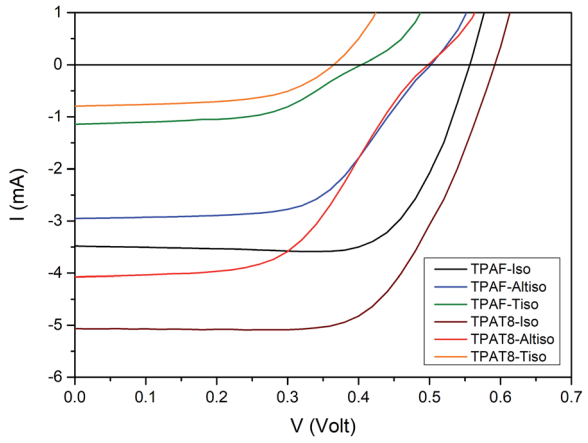

Fig. 3 *I–V* curves under 1 sun irradiation of DSSCs using the six dyes as sensitizers under optimized fabrication conditions.

To prove the reproducibility and reliability of our results, at least three optimized solar cells for each dye were fabricated and characterized under exactly the same conditions. The current–voltage characteristics of the best performing cells are given in Fig. 3; some of them clearly show a more or less pronounced S-shape which is unusual. A hypothesis to explain the origin of the S-shape is formulated in the next section. From the best-cell and average parameters summarized in Table 2, it appears that isoindigo-based dyes show the best performances, with a PCE of 4.01% and 5.84% for **TPAF-Iso** and **TPAT8-Iso**, respectively. This is mainly explained by the rather high J_{sc} (up to *circa* 15 mA cm^{-2}) delivered by these solar cells and the absence of the S-shape in the *I–V* curves that maintain the FF at high values. One should note here that these compounds led, however, to the lower dye-uptakes on the electrodes. The solar cells containing benzothieno-isoindigo-based dyes show rather similar PCE but the solar cells with **TPAT8-Altiso** lead to higher J_{sc}. Notably for these dyes, the V_{oc} is lower and the FF is strongly deteriorated by the S-shape of the *I–V* curve. Finally, the dyes containing thieno-isoindigo units show the worst performances, below 1%. The J_{sc} supplied by **TPAT8-Tiso** and **TPAF-Tiso** solar cells is extremely low despite that these devices exhibit the higher dye-loading and the larger absorption. As explained before, **TPAT8-Tiso** and **TPAF-Tiso** show a strong tendency to stack in the solid state. This phenomenon is known to provoke a photocurrent loss since the aggregates induce the quenching of the excited state of the dyes.[29] The IPCE curves show a trend that is comparable to the device performances and the photocurrent action spectra are all extended beyond 700 nm (see Fig. 4).

Photo-physical study of the solar cells

After measuring the *I–V* curves for all organic sensitizers in DSSCs using an iodine/iodide electrolyte, we observed that the

Table 2 Photovoltaic parameters of the solar cells obtained under the optimized fabrication conditions. Dyeing bath: dye/CDCA 0.2/10 mM, EtOH/$CHCl_3$ (4 : 1), electrodes: 12 + 4 μm, size 0.36 cm^2, electrolyte: BMII 0.5 M, I2 0.03 M, LiI 0.5 M, Gthio 0.5 M, *t*BP 0.1 M, irradiation 1 sun, using a mask. First lines correspond to the results of the best cells and the second lines correspond to the parameters obtained from three or four devices

Dye/CDCA	V_{oc} (V)	J_{sc} (mA cm^{-2})	FF	η (%)	Dye loading (mol cm^{-2})
TPAF-Iso	0.53	10.97	0.69	4.01	3.3×10^{-8}
	0.54 ± 0.02	10.09 ± 0.87	0.72 ± 0.03	3.88 ± 0.13	
TPAF-Altiso	0.47	9.69	0.59	2.66	7.0×10^{-8}
	0.5 ± 0.02	8.44 ± 1.18	0.60 ± 0.01	2.51 ± 0.19	
TPAF-Tiso	0.38	2.14	0.60	0.49	8.2×10^{-8}
	0.37 ± 0.02	1.90 ± 0.27	0.56 ± 0.06	0.41 ± 0.11	
TPAT8-Iso	0.59	14.55	0.68	5.84	4.3×10^{-8}
	0.57 ± 0.02	14.91 ± 1.23	0.65 ± 0.04	5.54 ± 0.49	
TPAT8-Altiso	0.50	11.28	0.53	2.99	9.9×10^{-8}
	0.48 ± 0.03	9.01 ± 1.44	0.59 ± 0.04	2.52 ± 0.29	
TPAT8-Tiso	0.38	3.33	0.55	0.70	13.0×10^{-8}
	0.38 ± 0.01	2.89 ± 0.53	0.55 ± 0.01	0.61 ± 0.12	

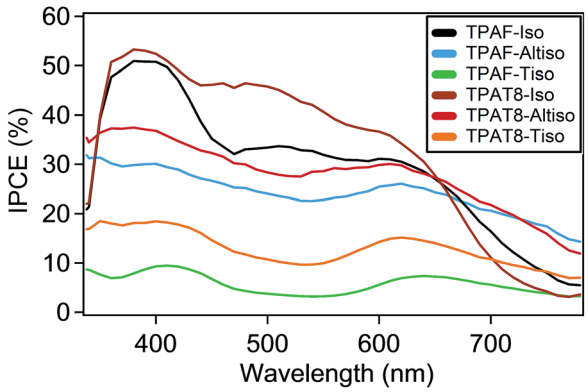

Fig. 4 IPCE spectra of the devices containing the six dyes.

photocurrent was strikingly low for some of the dyes. At first sight, one could think that this is due to difficulties related to the excited-state energy of the dyes with respect to the TiO_2 conduction band. However, both experimental results and theoretical experiments lead to the conclusion that the excited-states of the dyes are well above those of the TiO_2 conduction band. In fact, Laser Transient Absorption Spectroscopy (L-TAS) measurements shown later in this manuscript (Fig. 7) show efficient charge injection from the excited state of the dyes to the TiO_2 conduction band.

Hence, we analyzed in depth the photo-induced charge present in the solar cells for each dye in complete solar cells at different light intensities by using charge extraction, as reported previously.[30]

As shown in Fig. 5, the amount of charge is similar for all dyes at a given voltage close to the V_{oc} at 1 sun (for example for 0.5 V, the photo-induced charge density is 0.15×10^{18} electrons per cm^3). This value is among the normal values for DSSCs having dye coverages between 3 and 15×10^{-8} mol cm^{-2}. Thus, the differences seen in the IPCE and the measured photocurrent at short circuit (V_{oc} at 1 sun) must be due to a different reason but not due to the lack of efficient charge injection. Once the charge density was measured, we turned to analyze the carrier lifetime that is related to the recombination kinetics between the photo-injected electrons and the oxidized electrolyte. To do so, we have used the Transient Photo-Voltage (TPV) measurements that have been reported earlier.[31] Fig. 6 shows the measured lifetime *vs.* charge density for all the solar cells, which have been fabricated identically except for the different sensitizers used.

All carrier lifetimes (τ) fall in the millisecond time range (0.01–0.001 s) which is usual in DSSCs. However, the slope of the linear plots is quite different for **TPAF-Tiso**, which shows the lowest V_{oc} at 1 sun and a greater slope. The slope is related to the order of recombination kinetics, which clearly is much higher for **TPAF-Tiso** than for the other dyes. In fact, the trend follows quite well the V_{oc}; the solar cells with a higher slope, as **TPAT8-Tiso**, show a lower V_{oc} at 1 sun. Hence, from the TPV measurements we can correlate the observed differences in V_{oc} with the recombination kinetics (the order of the recombination kinetics) between the photo-injected electrons at TiO_2 and the oxidized electrolyte. Yet, we have not found a convincing explanation for the lower photocurrent measured for some dyes, in particular, **TPAF-Tiso** and **TPAT8-Tiso**. As mentioned above, neither **TPAF-Tiso** nor **TPAT8-Tiso** is limited by the nature of its excited state to inject electrons into TiO_2. Thus, we decided to study the interfacial charge injection and charge recombination kinetics of complete devices using L-TAS. For comparison purposes, we also measured solar cells made with **TPAT8-Iso** that show photocurrent as high as 15 mA cm^{-2} at 1 sun.

Fig. 7 shows the decay for each solar cell in the presence and absence of the electrolyte. As can be seen, for **TPAT8-Iso** and **TPAF-Iso**, and in absence of the electrolyte, the decay corresponds to the oxidized dye after efficient injection of electrons into TiO_2. The measured half-lifetime of the decay and the HWHM (Half Width at the Half Maximum) is 0.02 s. In contrast, in the presence of the iodine/iodide, the electrolyte fully regenerates the oxidized dye, the half-lifetime is of tenths of microseconds, and a slow phase is present that has been previously attributed to the I_3^- species.

For **TPAT8-Altiso**, the decay is slower. In clear contrast, for **TPAF-Tiso** and **TPAT8-Tiso**, the presence of the electrolyte does not regenerate the dye, and a slower decay is observed.

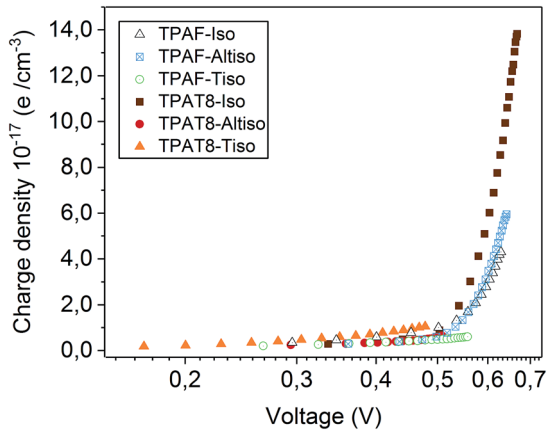

Fig. 5 Charge extraction data showing electron density as a function of the induced voltage for the different dyes.

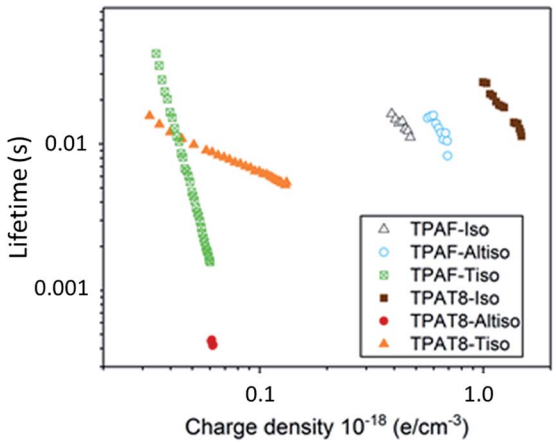

Fig. 6 Transient photovoltage (TPV) data showing electron lifetimes *versus* electron density for DSSC devices based on the six dyes.

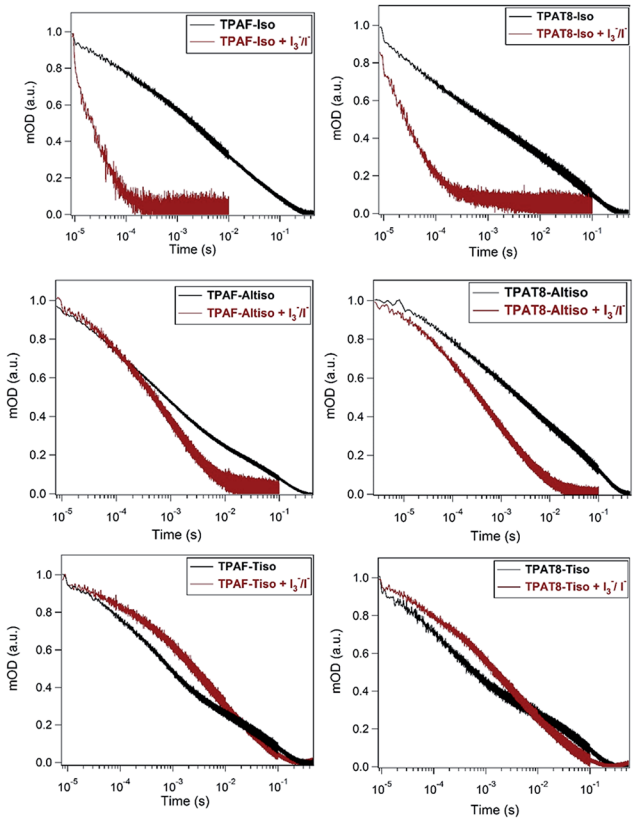

Fig. 7 L-TAS decay of the dyes anchored onto a TiO_2 film and in a complete device using the electrolyte.

A plausible explanation for this new decay trace might be the formation of a stable complex between the dye and the oxidized species of the electrolyte but this hypothesis is not confirmed by the theoretical calculations (*vide supra*). Another explanation could be that the regeneration is extremely slow for these dyes which are not fully regenerated. The hypothesis of an extremely slow regeneration processes is fully consistent with the low ΔE_{reg} values deduced from cyclic voltammetry measurements. This low driving force may cause the increase of the total series resistance of the DSSCs and could explain the low FF and the S-shape of the $I(V)$ curves observed for these devices. Indeed, a low FF is generally ascribed to high sheet resistance and/or a high series resistance in the device.[32]

However, to shed light on the results extracted from L-TAS experiments the interaction between iodide and the six dyes has been studied computationally (ESI†). The dyes have been optimized in acetonitrile in their neutral and radical cationic forms and the electrostatic potential (V_E) of the latter has been obtained (see Fig. 8). In Fig. 8, the surface in blue indicates the positively charged regions of the cationic radical dye, which should be the more favorable points for interacting with iodide.

As may be observed, the positively charged surface corresponds to the more hydrophobic regions, usually far away from the oxygen and sulfur atoms. We decided to compute two (or more, up to six for **TPAT8-Tiso** and **TPAT8-Iso**) different conformations for the interaction of each oxidized dye and the iodide, where the latter is placed close to the positively charged

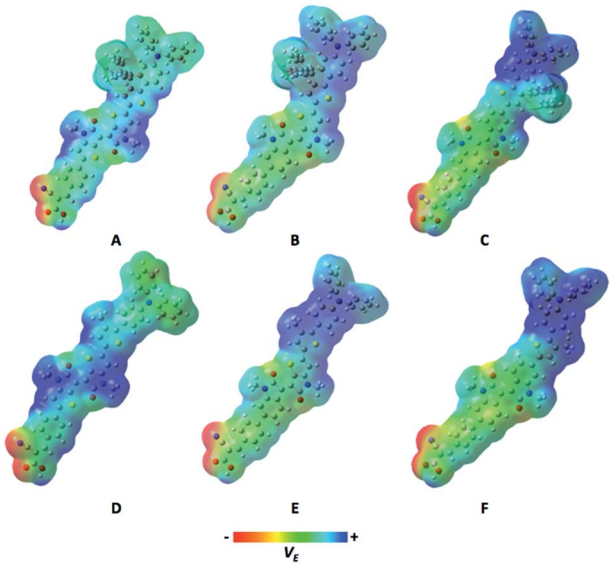

Fig. 8 Computed electrostatic potentials (V_E) for **TPAF-Tiso** (A), **TPAF-Altiso** (B), **TPAF-Iso** (C), **TPAT8-Tiso** (D), **TPAT8-Altiso** (E) and **TPAT8-Iso** (F). V_E ranges from −0.02 hartree (red) to +0.10 hartree (blue) over the total electron densities at an absolute isovalue of 0.02.

regions of the dye, namely terminal positively charged methyl, phenyl and hydrogen groups. For completion reasons, we also included all the S and O–S pockets as plausible anchoring points.

The calculations indicate that iodide does not interact strongly with any cationic radical dye; the most favorable interaction energy between both species (computed as the electronic energy difference between the dye^+–I^- complex and the separated species) falls in a range of −0.20 to −0.30 eV for all dyes (see Table S1 in the ESI†). In all the optimized dye^+–I^- complex structures, iodide moves around to find a more positively charged place to interact with, normally a terminal C–H bond (see Fig. S5 in the ESI†), with quite long distances in the range of 3.0–3.5 Å. These calculations seem to rule out the formation of stable complexes between the oxidized dye and iodide and thus the regeneration issues should be attributed to other reasons.

However, the more positively charged groups in **TPAF-Tiso** and **TPAT8-Tiso** being located closer to the anchoring function may favor the approach of the iodide closer to the TiO_2 surface thus leading to a higher recombination rate. This hypothesis is fully consistent with the higher recombination kinetics deduced from TPV measurements for these dyes, resulting in the lower V_{oc} values.

Finally, from the calculation we found that the z component of the dipole (see Table S1†) of the oxidized dyes is very different within the series of molecules, ranging from 78.58 to 132.51 debye. In 2005, Rühle and coworkers demonstrated that the V_{oc} of dye-sensitized solar cells varies linearly with the dipole moment of some co-adsorbed molecules used as additives to prevent aggregation of the dyes.[33] This result was explained in terms of a dipole-related shift of E_{CB} of the oxide.

This phenomenon was mostly observed using additive molecules, however the large variation of the dipole moments

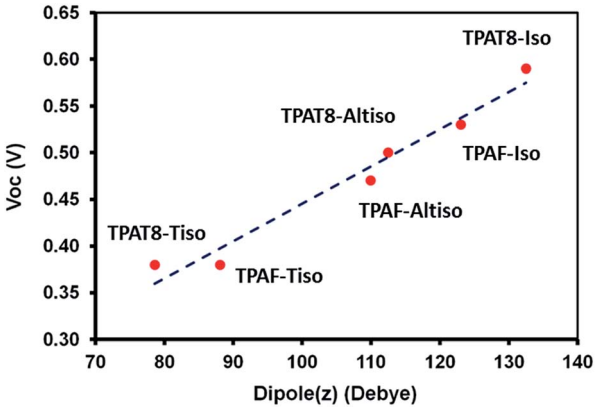

Fig. 9 Open-circuit voltage variation as a function of the dipole of the oxidized dyes.

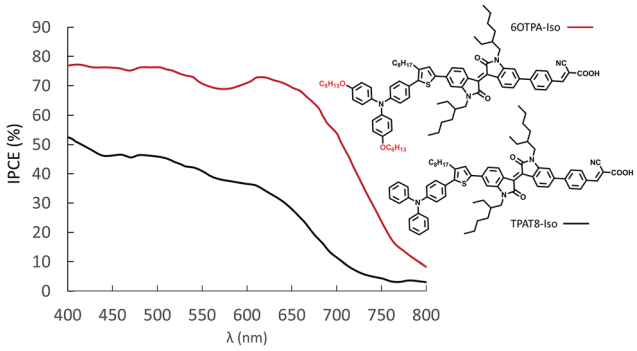

Fig. 10 Chemical structure of 6OTPA-Iso and comparison of the IPCE spectra of the devices containing TPAT8-Iso and 6OTPA-Iso dyes.

within our family of molecules could explain the large variations of the V_{oc} for the solar cells that we fabricated. To verify this hypothesis, the variation of the V_{oc} of the solar cells was plotted as a function of the dipole of the molecules, and the graph is presented in Fig. 9. We found a linear dipole dependence of the V_{oc} with the dipole of the dyes, similarly to the observation by Rühle and coworkers with co-adsorbent molecules,[33] the dye molecules possessing larger dipoles leading to higher open circuit voltages. This interesting observation could help chemists for designing molecules leading to higher V_{oc} in solar cells.

Perspectives of the work

Isoindigo-based dyes possess a high dipole in their oxidized state (>120 debye) and consequently lead to higher V_{oc} in solar cells. We demonstrated from the TAS experiments that these dyes can be regenerated efficiently by the electrolyte and the TPV experiments indicate that they lead to lower charge recombination rates. To highlight that our findings could drive the molecular design of more efficient dyes, we synthesized a new photosensitizer (coded as **6OTPA-Iso**) which is an analog of **TPAT8-Iso**. This molecule was synthesized in only four steps from the isoindigo unit using a modified TPA unit bearing hexyloxy chains. The introduction of alkoxy groups on the electron-donating unit of **TPAT8-Iso** is expected to produce a red-shift in the absorption spectrum[34] and to decrease further charge recombination,[35] as a consequence higher J_{sc} values are expected.[36] The chemical structure of this dye is presented in Fig. 10 and the synthetic route, and optoelectronic properties of this molecule are presented in the ESI.†

In dichloromethane solution, **6OTPA-Iso** shows a maximum wavelength of absorption in the visible region at 579 nm and an absorption edge located at 712 nm. The experimental determination of the energy levels (by CV and DPV) indicates a HOMO at −5.1 eV and a LUMO at −3.8 eV and DFT calculations confirm the appropriate localization of the HOMO and LUMO orbitals for good injection of electrons in TiO_2 (see the ESI†). Solar cells were fabricated using this photosensitizer and TiO_2 electrodes (a 12 μm-thick transparent layer and a 4 μm-thick scattering layer). After optimization of the *t*BP ratio in the electrolyte and the composition of the dyeing bath, a device with a maximum power conversion efficiency of 7.01% was obtained. The best device reaches a V_{oc} of 0.56 V and a FF of 0.64, but more interestingly a high J_{sc} of 19.4 mA cm^{-2} was obtained. The direct comparison of the IPCE spectra of **TPAT8-Iso** (the best dye from the previous series) and **6OTPA-Iso** based devices clearly indicates that the photocurrent response of the **6OTPA-Iso** device is significantly better at any wavelengths. Finally, the calculations carried out for this dye indicate that the oxidized form of **6OTPA-Iso** interacts weakly with iodide, which prefers coming close to the C–H bonds of the phenyl groups (Table S2 and Fig. S10 in the ESI†). The computed *z* component of the dipole for the cationic radical species of **6OTPA-Iso** is 135.1 D, in perfect agreement with the high V_{oc} value reached by the dye.

Conclusions

In conclusion, we investigated the potential of isoindigo, thieno-isoindigo or benzo-thieno-isoindigo chromophores to create organic dyes, absorbing in the UV-visible and near-infrared spectral range, for DSSC applications. Interestingly, some of the dyes showed absorption domains extended up to 900 nm. Devices based on **TPAT8-Iso** embedding an isoindigo central unit attained a PCE of *circa* 5.84%. Despite a panchromatic absorption and high absorption coefficients, some of the dyes based on thieno-isoindigo cores led to devices with poor performances with quite a low J_{sc}. Thanks to charge extraction, transient photovoltage, laser transient absorption spectroscopy experiments and computational investigations, we unravelled the interfacial processes that occurs with this family of dyes and we identified the detrimental processes that are responsible for the low performances. In particular, we demonstrated that thieno-isoindigo-based dyes exhibit higher charge recombination kinetics in solar cells principally because this chromophore unit modifies the electrostatic potential over the molecule allowing iodide to approach the TiO_2 surface. We also found that the dipole of the oxidized molecules plays a crucial role in the V_{oc} value, the dyes possessing larger dipoles leading to solar cells with higher open circuit voltages. Taking into account our conclusion regarding the structure–property relationship for

these dyes, we have synthesized a new photosensitizer based on the isoindigo core and the modified TPA unit to prevent recombination processes. This new panchromatic dye leads to devices with efficiency close to 7% associated with current densities above 19 mA cm^{-2} which ranks amongst the highest J_{sc} ever obtained for a NIR metal-free organic dye. This work unravel fundamental processes in DSSCs based on NIR dyes and could help to define new strategies of molecular engineering to develop more efficient organic dyes for DSSCs.

Conflicts of interest

There are no conflicts to declare.

Acknowledgements

The authors acknowledge financial support from the French Research Agency ANR (grants ANR ANR-14-OHRI-0003 ODYCE). E. P. and C. R. S. are also grateful to the Spanish Ministry of Economy and Competitiveness program (MINECO) for the CTQ2013-47183-R project. E. P. acknowledges the ICIQ and ICREA for financial support. R. D. acknowledges the LABEX Laboratoire d'Alliances Nanosciences-Energies du Futur (LANEF, ANR-10-LABX-51-44001) for funding and the Hybriden facility at CEA-Grenoble. C. A. acknowledges the University Grenoble Alpes for partial funding.

Notes and references

1 A. Hagfeldt, G. Boschloo, L. Sun, L. Kloo and H. Pettersson, *Chem. Rev.*, 2010, **110**, 6595–6663.

2 (*a*) Y. K. Eom, S. H. Kang, I. T. Choi, Y. Yoo, J. Kim and H. K. Kim, *J. Mater. Chem. A*, 2017, **5**, 2297–2308; (*b*) Z. Yao, H. Wu, Y. Li, J. Wang, J. Zhang, M. Zhang, Y. Guo and P. Wang, *Energy Environ. Sci.*, 2015, **8**, 3192–3197.

3 (*a*) D. Joly, L. Pelleja, S. Narbey, F. Oswald, J. Chiron, J. N. Clifford, E. Palomares and R. Demadrille, *Sci. Rep.*, 2014, **4**, 4033; (*b*) Q. Yu, D. Zhou, Y. Shi, X. Si, Y. Wang and P. Wang, *Energy Environ. Sci.*, 2010, **3**, 1722; (*c*) D. Joly, M. Godfroy, L. Pelleja, Y. Kervella, P. Maldivi, S. Narbey, F. Oswald, E. Palomares and R. Demadrille, *J. Mater. Chem. A*, 2017, **5**, 6122–6130.

4 (*a*) D. Joly, L. Pelleja, S. Narbey, F. Oswald, T. Meyer, Y. Kervella, P. Maldivi, J. N. Clifford, E. Palomares and R. Demadrille, *Energy Environ. Sci.*, 2015, **8**, 2010–2018; (*b*) A. Reale, L. Cin, A. Malatesta, R. De Marco, T. M. Brown and A. Di Carlo, *Energy Technol.*, 2014, **2**, 531–541.

5 C.-Y. Chen, M. Wang, J.-Y. Li, N. Pootrakulchote, L. Alibabaei, C. Ngoc-le, J.-D. Decoppet, J.-H. Tsai, C. Grätzel, C.-G. Wu, S. M. Zakeeruddin and M. Grätzel, *ACS Nano*, 2009, **3**, 3103–3109.

6 (*a*) L.-L. Li and E. W.-G. Dia, *Chem. Soc. Rev.*, 2013, **42**, 291–304; (*b*) A. Yella, H.-W. Lee, H. N. Tsao, C. Yi, A. K. Chandiran, M. K. Nazeeruddin, E. W.-G. Diau, C.-Y. Yeh, S. M. Zakeeruddin and M. Grätzel, *Science*, 2011, **334**, 629–634; (*c*) S. Mathew, A. Yella, P. Gao, R. Humphry-Baker, B. F. E. Curchod, N. Ashari-Astani, I. Tavernelli, U. Rothlisberger, M. K. Nazeeruddin and M. Grätzel, *Nat. Chem.*, 2014, **6**, 242.

7 (*a*) X. Li, Y. Hu, I. Sanchez-Molina, Y. Zhou, F. Yu, S. A. Haque, W. Wu, J. Hua, H. Tian and N. Robertson, *J. Mater. Chem. A*, 2015, **3**, 21733–21743; (*b*) Y. Gao, X. Li, Y. Hu, Y. Fan, J. Yuan, N. Robertson, J. Hua and S. R. Marder, *J. Mater. Chem. A*, 2016, **4**, 12865–12877.

8 (*a*) Q. Chai, W. Li, J. Liu, Z. Geng, H. Tian and W. H. Zhu, *Sci. Rep.*, 2015, **5**, 11330; (*b*) Y. Ren, Y. Li, S. Chen, J. Liu, J. Zhang and P. Wang, *Energy Environ. Sci.*, 2016, **9**, 1390–1399; (*c*) Z. Wu, X. Li, J. Li, H. Ågren, J. Hua and H. Tian, *J. Mater. Chem. A*, 2015, **3**, 14325–14333.

9 J.-H. Yum, T. W. Holcombe, Y. Kim, K. Rakstys, T. Moehl, J. Teuscher, J. H. Delcamp, M. K. Nazeeruddin and M. Grätzel, *Sci. Rep.*, 2013, **3**, 2446.

10 (*a*) M. García-Iglesias, J.-H. Yum, R. Humphry-Baker, S. M. Zakeeruddin, P. Péchy, P. Vázquez, E. Palomares, M. Grätzel, M. K. Nazeeruddin and T. Torres, *Chem. Sci.*, 2011, **2**, 1145–1150; (*b*) J.-J. Cid, J.-H. Yum, S.-R. Jang, M. K. Nazeeruddin, E. Martinez-Ferrero, E. Palomares, J. Ko, M. Grätzel and T. Torres, *Angew. Chem., Int. Ed.*, 2007, **46**, 8358–8362; (*c*) J.-J. Cid, M. Garcia-Iglesias, J.-H. Yum, A. Forneli, J. Albero, E. Martinez-Ferrero, P. Vazquez, M. Grätzel, M. K. Nazeeruddin, E. Palomares and T. Torres, *Chem.–Eur. J.*, 2009, **15**, 5130–5137; (*d*) L. Martin-Gomis, F. Fernandez-Lazaro and A. Sastre-Santos, *J. Mater. Chem. A*, 2014, **2**, 15672–15682.

11 (*a*) S. Paek, H. Choi, C. Kim, N. Cho, S. So, K. Song, M. K. Nazeeruddin and J. Ko, *Chem. Commun.*, 2011, **47**, 2874–2876; (*b*) Y. Adachi, Y. Ooyama, N. Shibayama and J. Ohshita, *Chem. Lett.*, 2017, **46**, 310–312; (*c*) A. Islam, T. H. Chowdhury, C. Qin, L. Han, J.-J. Lee, I. M. Bedja, M. Akhtaruzzaman, K. Sopian, A. Mirloup and N. Leclerc, *Sustainable Energy Fuels*, 2018, **2**, 209–214; (*d*) S. Yamamoto, T. Ikeuchi, S. Mori and M. Kimura, *Asian J. Org. Chem.*, 2014, **3**, 1083–1088; (*e*) D. Arteaga, R. Cotta, A. Ortiz, B. Insuasty, N. Martin and L. Echegoyen, *Dyes Pigm.*, 2015, **112**, 127–137.

12 (*a*) T. Ikeuchi, H. Nomoto, N. Masaki, M. J. Griffith, S. Mori and M. Kimura, *Chem. Commun.*, 2014, **50**, 1941–1943; (*b*) Y. Kubo, D. Eguchi, A. Matsumoto, R. Nishiyabu, H. Yakushiji, K. Shigaki and M. Kaneko, *J. Mater. Chem. A*, 2014, **2**, 5204–5211.

13 T. Lei, J.-Y. Wang and J. Pei, *Acc. Chem. Res.*, 2014, **47**, 1117–1126.

14 W. Ying, F. Guo, J. Li, Q. Zhang, W. Wu, H. Tian and J. Hua, *ACS Appl. Mater. Interfaces*, 2012, **4**, 4215–4224.

15 (*a*) D. Wang, W. Yin, X. Zhang, Y. Hu, W. Wu and J. Hua, *Dyes Pigm.*, 2015, **112**, 327–334; (*b*) S.-G. Li, K.-J. Jiang, J.-H. Huang, L.-M. Yang and Y.-L. Song, *Chem. Commun.*, 2014, **50**, 4309.

16 M. S. Chen, J. R. Niskala, D. A. Unruh, C. K. Chu, O. P. Lee and J. M. J. Fréchet, *Chem. Mater.*, 2013, **25**, 4088–4096.

17 R. Stalder, J. Mei and J. R. Reynolds, *Macromolecules*, 2010, **43**, 8348–8352.

18 (*a*) W. Zhang, Y. Wu, H. Zhu, Q. Chai, J. Liu, H. Li, X. Song and W.-H. Zhu, *ACS Appl. Mater. Interfaces*, 2015, **7**, 26802–

26810; (*b*) Z.-S. Wang and H. Sugihara, *Langmuir*, 2006, **22**, 9718–9722; (*c*) M. Wielopolski, M. Marszalek, F. G. Brunetti, D. Joly, J. Calbo, J. Arago, J.-E. Moser, R. Humphry-Baker, S. M. Zakeeruddin, J. L. Delgado, M. Gratzel, E. Orti and N. Martin, *J. Mater. Chem. C*, 2016, **4**, 3798–3808.

19 (*a*) Z.-S. Wang, N. Koumura, Y. Cui, M. Takahashi, H. Sekiguchi, A. Mori, T. Kubo, A. Furube and K. Hara, *Chem. Mater.*, 2008, **20**, 3993–4003; (*b*) L. Zhang and J. M. Cole, *J. Mater. Chem. A*, 2017, **5**, 19541–19559.

20 (*a*) C. Fiolhais, F. Nogueira and M. A. Marques, *A primer in density functional theory*, Springer Science & Business Media, 2003, vol. 620, pp. 218–256; (*b*) K. Burke and L. O. Wagner, *Int. J. Quantum Chem.*, 2013, **113**, 96–101.

21 G. Zhang and C. B. Musgrave, *J. Phys. Chem. A*, 2007, **111**, 1554–1561.

22 (*a*) L. A. Estrada, R. Stalder, K. A. Abboud, C. Risko, J.-L. Brédas and J. R. Reynolds, *Macromolecules*, 2013, **46**, 8832–8844; (*b*) A. Ganguly, J. Zhu and T. L. Kelly, *J. Phys. Chem. C*, 2017, **121**, 9110–9119.

23 (*a*) J. Casado, M. Z. Zgierski, P. C. Ewbank, M. W. Burand, D. E. Janzen, K. R. Mann, T. M. Pappenfus, A. Berlin, E. Pérez-Inestrosa, R. P. Ortiz and J. T. López Navarrete, *J. Am. Chem. Soc.*, 2006, **128**, 10134–10144; (*b*) J. Casado, T. M. Pappenfus, L. L. Miller, K. R. Mann, E. Ortí, P. M. Viruela, R. Pou-Amérigo, V. Hernández and J. T. López Navarrete, *J. Am. Chem. Soc.*, 2003, **125**, 2524–2534; (*c*) G. E. Rudebusch, J. L. Zafra, K. Jorner, K. Fukuda, J. L. Marshall, I. Arrechea-Marcos, G. L. Espejo, R. Ponce Ortiz, C. J. Gómez-García, L. N. Zakharov, M. Nakano, H. Ottosson, J. Casado and M. M. Haley, *Nat. Chem.*, 2016, **8**, 753–759.

24 M. Grätzel, *Acc. Chem. Res.*, 2009, **42**, 1788–1798.

25 G. Boschloo and A. Hagfeldt, *Acc. Chem. Res.*, 2009, **42**, 1819–1826.

26 (*a*) J. Preat, D. Jacquemin and E. A. Perpète, *Energy Environ. Sci.*, 2010, **3**, 891–904; (*b*) A. Hagfeldt, G. Boschloo, L. Sun, L. Kloo and H. Pettersson, *Chem. Rev.*, 2010, **110**, 6595–6663; (*c*) M. Godfroy, C. Aumaitre, F. Caffy, Y. Kervella, L. Cabau, L. Pelleja, P. Maldivi, S. Narbey, F. Oswald, E. Palomares, D. Joly and R. Demadrille, *Dyes Pigm.*, 2017, **146**, 352–360.

27 R. Stalder, D. Xie, A. Islam, L. Han, J. R. Reynolds and K. S. Schanze, *ACS Appl. Mater. Interfaces*, 2014, **6**, 8715–8722.

28 (*a*) S. E. Koops, B. C. O'Regan, P. R. F. Barnes and J. R. Durrant, *J. Am. Chem. Soc.*, 2009, **131**, 4808–4818; (*b*) G. Boschloo, L. Häggman and A. Hagfeldt, *J. Phys. Chem. B*, 2006, **110**, 13144–13150; (*c*) J. Wu, Z. Lan, J. Lin, M. Huang, Y. Huang, L. Fan and G. Luo, *Chem. Rev.*, 2015, **115**, 2136–2173.

29 S. Tatay, S. A. Haque, B. O'Regan, J. R. Durrant, W. J. H. Verhees, J. M. Kroon, A. Vidal-Ferran, P. Gavina and E. Palomares, *J. Mater. Chem.*, 2007, **17**, 3037–3044.

30 P. R. F. Barnes, K. Miettunen, X. Li, A. Y. Anderson, T. Bessho, M. Grätzel and B. C. O'Regan, *Adv. Mater.*, 2013, **25**, 1881–1922.

31 (*a*) L. Pelleja, C. V. Kumar, J. N. Clifford and E. Palomares, *J. Phys. Chem. C*, 2014, **118**, 16504–16509; (*b*) B. C. O'Regan, K. Bakker, J. Kroeze, H. Smit, P. Sommeling and J. R. Durrant, *J. Phys. Chem. B*, 2006, **110**, 17155–17160; (*c*) T. Zewdu, J. N. Clifford, J. Pérez Hernández and E. Palomares, *Energy Environ. Sci.*, 2011, **4**, 4633–4638.

32 (*a*) J.-H. Yum, T. W. Holcombe, Y. Kim, K. Rakstys, T. Moehl, J. Teuscher, J. H. Delcamp, M. K. Nazeeruddin and M. Grätzel, *Sci. Rep.*, 2013, **3**, 2446; (*b*) F. Fabregat-Santiago, J. Bisquert, E. Palomares, L. Otero, D. Kuang, S. M. Zakeeruddin and M. Grätzel, *J. Phys. Chem. C*, 2007, **111**, 6550–6560.

33 S. Rühle, M. Greenshtein, S.-G. Chen, A. Merson, H. Pizem, C. S. Sukenik, D. Cahen and A. Zaban, *J. Phys. Chem. B*, 2005, **109**, 18907–18913.

34 Z. Ning and H. Tian, *Chem. Commun.*, 2009, 5483.

35 (*a*) Z. Ning, Y. Fu and H. Tian, *Energy Environ. Sci.*, 2010, **3**, 1170; (*b*) M. Xu, R. Li, N. Pootrakulchote, D. Shi, J. Guo, Z. Yi, S. M. Zakeeruddin, M. Grätzel and P. Wang, *J. Phys. Chem. C*, 2008, **112**, 19770.

36 (*a*) Y. Ooyama and Y. Harima, *Eur. J. Org. Chem.*, 2009, 2903; (*b*) Y. Ooyama and Y. Harima, *ChemPhysChem*, 2012, **13**, 4032.